A numerical study of the impact perforation of sandwich panels with graded hollow sphere cores

Ibrahim Elnasri, Han Zhao

Research Article

A numerical study of the impact perforation of sandwich panels with graded hollow sphere cores

Ibrahim Elnasri[1,2] [ID] and Han Zhao[3,4]

Abstract

In this study, we numerically investigate the impact perforation of sandwich panels made of 0.8 mm 2024-T3 aluminum alloy skin sheets and graded polymeric hollow sphere cores with four different gradient profiles. A suitable numerical model was conducted using the LS-DYNA code, calibrated with an inverse perforation test, instrumented with a Hopkinson bar, and validated using experimental data from the literature. Moreover, the effects of quasi-static loading, landing rates, and boundary conditions on the perforation resistance of the studied graded core sandwich panels were discussed. The simulation results showed that the piercing force–displacement response of the graded core sandwich panels is affected by the core density gradient profiles. Besides, the energy absorption capability can be effectively enhanced by modifying the arrangement of the core layers with unclumping boundary conditions in the graded core sandwich panel, which is rather too hard to achieve with clumping boundary conditions.

Introduction

Impact behavior (i.e. energy absorption, perforation resistance) is an important design feature in sandwich panels, which are used in aeronautic structures. Sandwich panels are usually made of two thin, stiff face sheets, often made of aluminum or a composite, and a thick, low-density core.

The assessment of such components in penetration/perforation resistance at high impact velocity has been mainly relied on experimental tests, and over the last decade a considerable number of numerical models have also been developed. Two techniques of assessment have been reported in the open literature: (i) the free-flying penetrator–immobile-target testing scheme[1–3] and (ii) the inverse perforation testing technique.[4] The first method is considered to be the most widely used, and it aims to determine the ballistic limit velocity curves. The second method aims at a high-quality force–displacement curve record during the whole perforation process, which represents a weak point of the first technique. Several researchers have reported numerous combined experimental and numerical studies or only numerical models focusing on understanding the perforation resistance of sandwich panels/advanced composites under quasi-static and impact loading.[5–11]

[1]Laboratoire de Génie Mécanique. Ecole Nationale d'Ingénieurs de Monastir, University of Monastir, Monastir, Tunisia
[2]Faculty of Engineering, University of Tabuk, Tabouk, Kingdom of Saudi Arabia
[3]Laboratoire de Mécanique et Technologie, ENS Paris-Saclay/CNRS, Gif-sur-Yvette, France
[4]Sorbonne Université, UFR 919, Paris Cedex 05, France

Corresponding author:
Ibrahim Elnasri, Faculty of Engineering, University of Tabuk, P.O. Box 741, Tabouk 71471, Kingdom of Saudi Arabia.
Email: Ibrahim.nasri@issig.rnu.tn

One of the most important problems in sandwich panels is the damage that occurs as a result of the discontinuity of the mechanical properties at the boundary between the face sheets and the core. When these sandwiches are exposed to impact loading, for example, the shear stresses can cause the face sheets to detach from the core. Over the past few decades, functionally graded material (FGM) cores have increasingly been used in sandwich panels because of their ability to reduce thermal and residual stresses induced between the face sheets and core material in comparison to conventional sandwich panels.[12] Such graded properties arise from different geometrical parameters, such as the diameter, width, and wall thickness and they also result from variable material properties, including the density, strength, and even material type.[13] Currently, different manufacturing techniques are used to manufacture core materials with graded properties.[14,15]

Various numerical and experimental studies have investigated the impact response of functionally graded foam sandwich panels. However, there has been no consensus regarding whether graded core sandwich panels have better perforation resistance than ungraded core sandwich panels with equal mass. Some researchers have pointed out that graded core sandwich panels can outperform ungraded ones in terms of the absorption energy,[16,17] although others have found that graded core sandwich panels may have worse perforation resistance[18–20] or may be even useless under quasi-static loading.[21] In recent years, considerable research efforts have been made to examine the impact behavior of functionally graded foam cores with polymeric hollow spheres,[22,23] metallic hollow spheres,[24] and metallic foams.[25] Most of the previous studies have focused on the introduction of a proprietary gradient that can vary the general response of FGM structures with certain optimization of the arrangement of the gradient profiles. From a theoretical study's perspective, some constitutive models have recently been reported in the literature to model the behavior of layered graded foams under quasi-static and impact loading, such as the mesoscopic model;[26] shock model;[27] elastic, collapse, plastic-hardening, densification constitutive model;[28] and elastic, plastic-hardening, locking model.[29]

The aim of this study is to provide insights into the impact perforation of sandwich panels made of 0.8 mm 2024-T3 aluminum alloy skin sheets and graded polymeric hollow sphere cores. Four gradient profiles were taken as a reference: A-4321, B-1234, D-2431, and E-4123. The four numbers constituting the names of these profiles signify the sequence of the layer's density beginning from the top skin. A-4321 (B-1234) signify then linearity decreasing (increasing) graded hollow spheres cores. The D-2431 gradient profile is a profile with an unbalanced V-shape with a few dense ends, whereas the E-4123 gradient profile has an unbalanced V-shape with more dense ends.

The remainder of this paper is organized as follows. Section 2 presents the problem statement. Section 3 describes the numerical model of the impact perforation of graded core sandwich panels with the LS-DYNA code, including finite element modeling, constitutive material modeling of aluminum sheets and graded cores, and validation of the proposed numerical approach. The presentation of virtual test results under perforation loading will be shown in Section 4. In the last section, the effects of quasi-static loading, loading rates, and boundary conditions on the perforation resistance of the studied graded core sandwich panels are discussed. A comparison of the specific perforation resistance of these graded core sandwich panels with other sandwich panel constructions with different cellular material cores is also provided at the end of the section.

Problem statement

In this numerical study, sandwich panels with a diameter of 60 mm, made of two 0.8 mm 2024-T3 aluminum alloy skin sheets and a core with polymeric hollow spheres of 40 mm, were used to model the impact perforation of sandwich panels with FGMs. Table 1 lists the basic characteristics of the graded core sandwich samples. Gradient profiles were obtained by changing the hollow spheres' density every 10 mm. The density of the layers was considered to be in the range of 156 to 468 kg/m^3.

To validate the numerical simulation results, the density of each layer was chosen to match that of the

Table 1. Basic characteristics of the graded core sandwich samples.

Reference sandwich (kg/m^3)	Core density	First layer density	Second layer density	Third layer density	Fourth layer density
A-4321 (sandwich)	302	468	343	242	156
B-1234 (sandwich)	302	156	242	343	468
D-2431 (sandwich)	302	343	468	242	156
E-4123 (sandwich)	302	468	156	343	242

Table 2. Input material parameters for the four polymeric hollow sphere core layers.

	Dimensions (mm^2)	Density (kg/m^3)	Elastic modulus in uncompressed configuration (MPa)	Yield stress for uncompressed configuration (MPa)	Elastic modulus for fully compacted material (GPa)	Yield stress for fully compacted material (MPa)	Densification strain	Tensile strain at failure
First layer	Φ40×10	468	1900	8	6	60	0.5	0.1
Second layer	Φ40×10	343	1500	5.5	6	60	0.7	0.1
Third layer	Φ40×10	242	1000	2.95	6	60	0.75	0.1
Four layer	Φ40×10	156	500	0.8	6	60	0.8	0.1

sample in the experimental research performed by Zeng et al.[21] In that study, no experimental results were obtained for the impact perforation of such graded core sandwich panels with intermediary gradient profiles: D-2431 and E-4123. In addition, they only simulated the perforation of the top skin because the used foam like constitutive model with volumetric strain failure criteria does not capture accurately the failure mode.
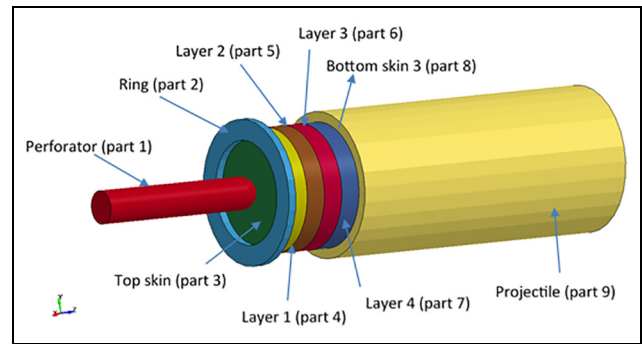
An inverse perforation technique with Hopkinson pressure bars was used to study graded core sandwich panels under impact loading. The sample was shot with the support of a hollow tube-like bullet against a long instrumented Hopkinson bar. Circular sandwich samples were clumped between the open end of the tube-like bullet and an aluminum-clumping ring, and six uniformly distributed bolts were slightly tightened to provide fixture. An impact velocity of 45 m/s was used in all tests. To read about the theory behind such an experimental setup, please refer to Zhao et al.[4]

As it is expensive to perform extra experiments and no detailed local information was available because of some experimental difficulties, a numerical analysis was necessary to provide more insights into better understanding the perforation process of graded core sandwich panels., see Table 2 for Input material parameters for the four polymeric hollow sphere core layers.

Numerical model of the impact perforation of graded core sandwich panels

Finite element modeling

In this study, we developed a numerical model of the perforation of sandwich panels with graded cores using the explicit finite element LS-DYNA code. The model consisted of two aluminum skin sheets and a graded core, with the core comprising four layers with different densities. As shown in Figure 1, the model consisted of nine parts.

Figure 1. Numerical model for the perforation of a graded core sandwich panel, testing configuration.

Part 1 (perforator) is represented as an elastic type 1 material. Part 9 (aluminum hollow tube-like bullet) and Part 2 (ring) are modeled as rigid bodies with type 20 material. These rigid parts (bullet and ring) are merged into a single component using the LS-DYNA keyword *CONSTRAINED_RIGID_BODIES. The 2024-T3 aluminum sheets are modeled by shell elements with five integration points in thickness, and the four graded layers are modeled using brick elements. This model consists of 421,107 nodes with 393,656 3D elements (33,536 for the perforator, 360,000 for the four graded layers, and 120 for the rigid parts) and 12,000 2D elements for the aluminum skin sheets.

The sandwich panels were modeled with a fine mesh in the penetration area just under the perforator. Shell elements with dimensions of 0.467×0.467 mm were used for the aluminum skin sheets. Each layer was modeled using brick elements with dimensions of $0.467 \times 0.467 \times 0.666$ mm. All dimensions were chosen on the basis of a trade-off between various mesh sizes (no significant mesh dependence was observed). Tie constraints were applied between the top skin and the first layer (Part 4) and between the bottom skin and the last layer (Part 7). Contact between the layers was obtained by merging the nodes between the layers. Contact between the Split Hopkinson pressure perforator bar and the sandwich panels was defined using

eroding surface-to-surface contact. The contact between the face skin and the layers after failure was modeled as eroding single surface contact. A segment-based contact option was defined to simulate the sandwich panel impact, and frictionless contact was assumed. All the parts in this work were modeled with a single integration point because reduced integration elements are considered (a robust choice for nonlinear analyses to control negative volumes in layers). However, reduced integration elements often suffer from hourglass modes. Therefore, a hourglass control (type 4 control) card was defined to control this non-physical behavior. All z-translational and z-rotational degrees of freedom in the no-loading end of the Hopkinson bar were fixed. Contact "tied" was defined between the sandwich panel and the two clumping parts. The velocities of the sample and the bullet were modeled and input as initial velocity nodes.

Modeling of the aluminum skin sheet

The behavior of the skin sheet was modeled using the constitutive material model proposed by Lemaitre,[30] available in the LS-DYNA code as a type 104 model. Such an isotropic damage model proposes a relationship between effective stress and damage-accumulated plastic strain, moderated by an isotropic damage variable. The parameters used for the 2024-T3 aluminum sheets were identified from the normalized tension tests by Pattofatto et al.[6] The following material data were used: $\rho = 2700 \, \text{kg/m}^3$, $E = 70 \, \text{GPa}$, $\upsilon = 0.3$, $Y = 364.5 \, \text{MPa}$, $Q_1 = 227.7 \, \text{MPa}$, $Q_2 = 0 \, \text{MPa}$, $C_1 = 3.3798$, $C_2 = 0$, $r_D = 0.23$, $S = 0.5 \, \text{MPa}$, and $D_c = 0.6$.

Modeling of the hollow graded core

The four layers with different densities were represented by a simple material model *MAT_HONEYCOMB, which has been specifically developed for honeycomb and foam materials. Such a selection was sparked by the simplicity of the model and it does account for erosion, which is necessary for modeling failure in such an impact perforation problem. The polymeric hollow sphere layers used in this study were considered to be isotropic; therefore, the input material parameters for the constitutive model for each layer were the same in the three orthogonal directions. Curves of normal stress versus volumetric strain for different density foams were obtained from the quasi-static compression tests performed by Zeng et al.[23] As it is difficult to obtain accurate shear testing results for such brittle hollow spheres, the shear stress versus volumetric strain curve was just supposed to satisfy the Tresca criterion at any volume strain level. Fracture of the cell of the hollow sphere layers was achieved by setting a tensile failure

strain. Table 2 lists the constitutive properties of the four-layer core.

Validation of the numerical simulation

Using the aforementioned constitutive models, a simulation of a piercing test of sandwich panels with A-4321 and B-1234 gradient profiles at 45 m/s was performed first to validate the numerical approach with the experimental results obtained by Zeng et al.[21] The simulation results were compared with the experimental data in terms of the piercing force–displacement response. The piercing force was obtained using the database nodal force group. All nodes on the piercing end were incorporated in the group nodes, which can be compared with the piercing force recorded using the strain gauge cemented on the split Hopkinson pressure bar. Figure 2(a) compares the curves of the impact force versus displacement obtained from both the experiment and simulation for graded core sandwich panels with a decreasing gradient profile (A-4321). It can be seen that the trends of simulated force–displacement responses agree well with the experimental results. The numerical model predicts the peak forces for the perforation of the top and bottom skins with a high degree of accuracy in comparison to the measured piercing forces. However, as illustrated in Figure 2(b), a discrepancy of the simulated piercing force versus displacement curve of graded core sandwich panels with an increasing gradient profile (B-1234) with the experimental results was observed. It can be observed that the numerical model does not capture all of the main features of the experiments.

Moreover, in the numerical results, it can also be seen that the two typical piercing peaks forces correspondence to the perforation of the top and bottom skin sheets separated by a long increase piercing forces phase corresponding to the perforation of gradient layers. However, in the experimental results,[21] the top skin sheet was not pierced before a displacement of 30 mm. This discrepancy is probably due to the difference between the experimental and numerical boundary conditions. Indeed, the contact between the ring and the top skin was constrained in the numerical model. Consequently, the contact surfaces cannot detach between them during the perforation loading and make the virtual test configuration performed with clumping boundary conditions. Nevertheless, in the experimental setup, the sample was sandwiched between the ring and the projectile by six uniformly distributed, slightly tightened bolts. Such contact between the ring and the top skin may detach during perforation loading in particular if the weak layer is placed in contact with the top skin. Hence, it was not possible to reach clumping boundary conditions in the experimental test configuration, causing the top skin to fold and never become perforated.
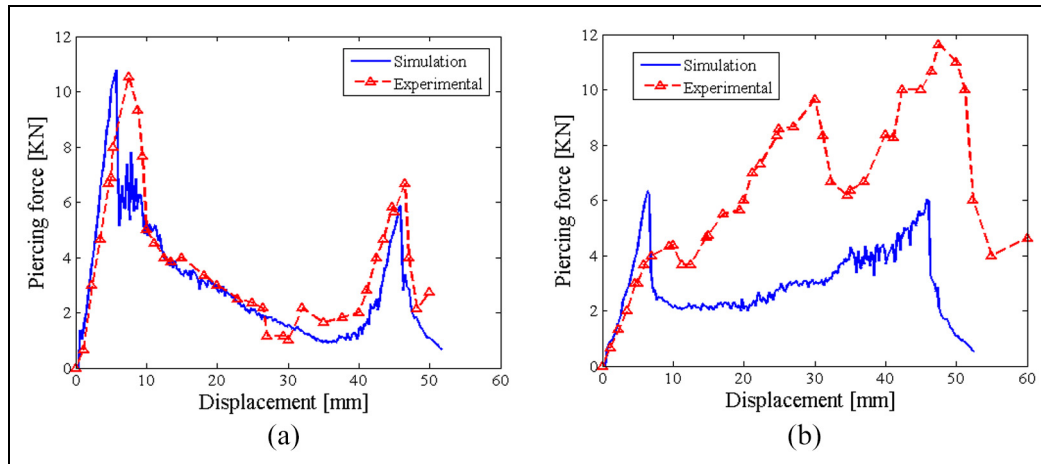
Figure 2. Plots of piercing force versus displacement of graded core sandwich panels. Comparison between the simulation and experimental results.[21] Sandwiches with the gradient profiles (a) A-4321 and (b) B-1234.
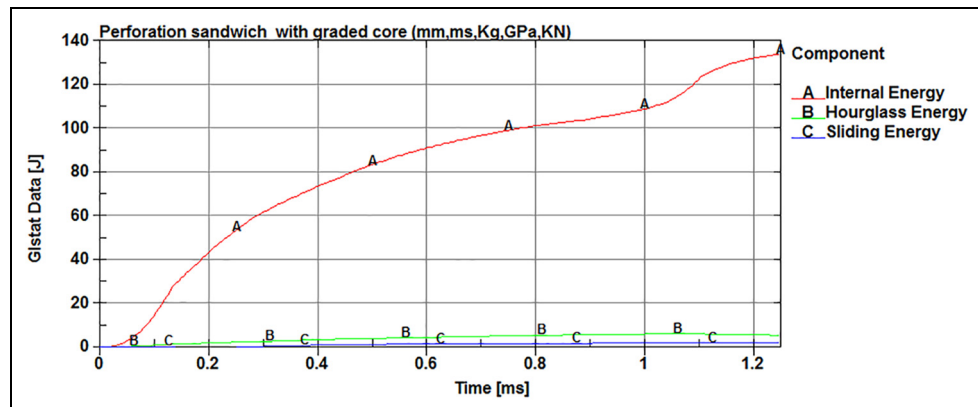

Figure 3. Plots of energy balance in the computational model. Graded core sandwich with the gradient profile A-4321 ($v = 45$ m/s).

From a purely numerical viewpoint, the hourglass energy arising from the use of reduced integration elements and the sliding energy due to the contact condition should be checked. In general, the hourglass energy should not be less than 10% of the internal energy, and the sliding energy should be positive.[31] Figure 3 shows the energy balance of this virtual test of graded core sandwich panels with a decreasing gradient profile. The results indicate that the energy balance is reliable. According to the results outlined above, we believe that the predictability of the proposed numerical approach is reliable in general.

Results

Impact perforation results

All the force–displacement curves of all graded core sandwich panels are shown in Figure 4. It was found that the force–displacement response is affected by the core density gradient. More specifically, A-4321 has the highest incident piercing top skin peak force, followed
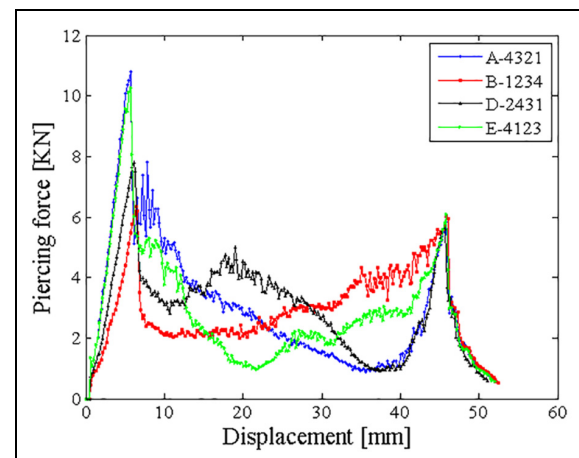

Figure 4. Plots of simulated piercing force versus displacement. Comparison between graded core sandwich panels at an impact velocity of 45 m/s.

by E-4123, D-2431, and B-1234, when comparing the peak force for the perforation of the top skin sheet. On
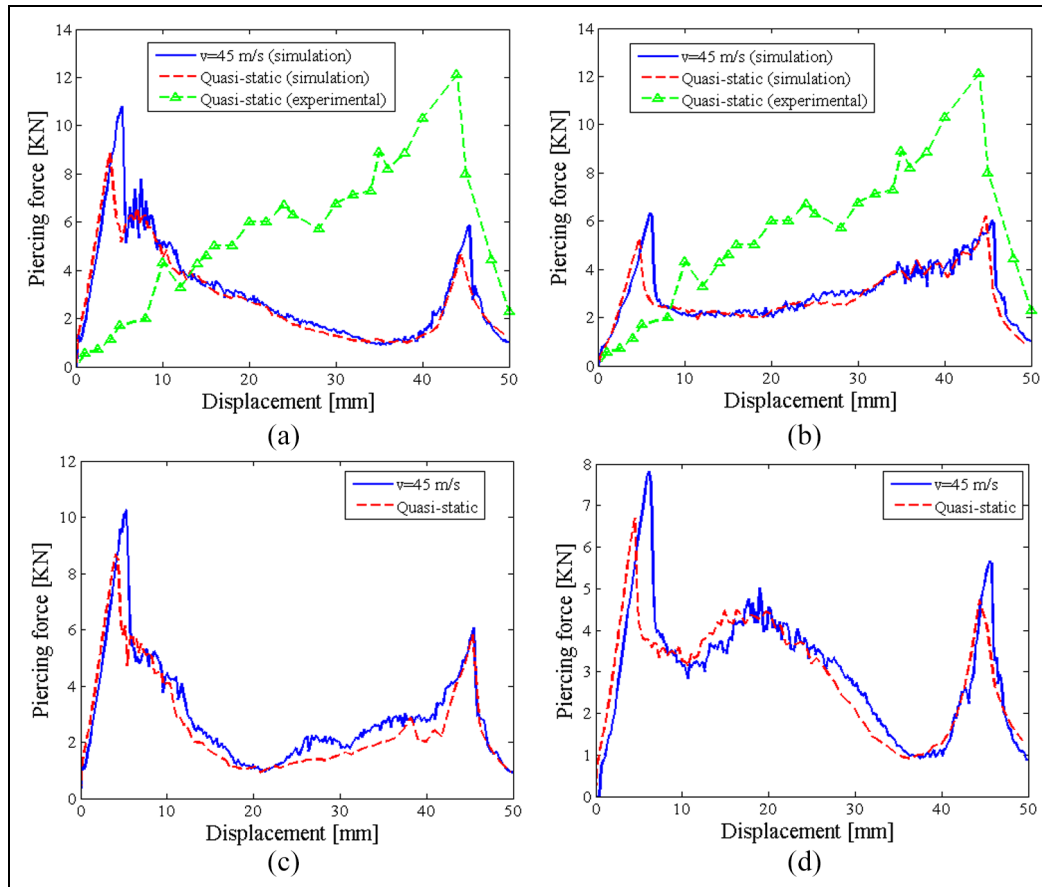
Figure 5. Plots of quasi-static and impact simulated piercing force versus displacement. Comparison between different graded core sandwich panels. Sandwiches with the gradient profiles: (a) A-4321, (b) B-1234, (c) E-4123, and (d) D-2431.

the other hand, the piercing bottom skin peak force, which is independent of the core density, has the same peak force value for all graded core sandwich panels, which is presumed to be the piercing force for single skin sheets. It can also be seen that both the top and bottom skins are broken at the same displacement for all graded core sandwich panels. After the first peak, the piercing force curves decreased with the increase in displacement corresponding to the perforation of the layers. These results indicate that the gradient profiles significantly affect the piercing force–displacement curves of graded core layers.

Quasi-static perforation results

It should be noted that the configuration of the quasi-static simulations was the same as that of the impact simulation and that the perforator was fixed with the same boundary conditions. To ensure quasi-static loading, we used the prescribed velocity field suggested by Hanssen et al.[32] The velocity of the projectile was modeled using the keyword *BOUDARY_PRESCRIBED_ MOTION_RIGID, and the velocities of the foam and

all nodes on the interface in contact with the projectile were modeled using the keyword *BOUNDARY_ PRESCRIBED_MOTION_NODE.

Figure 5(a) and (b) show the results of the perforation simulations in quasi-static graded core sandwich panels with increasing and decreasing gradient profiles, namely, A-4321 and B-1234, respectively. However, these simulations did not match the main features of the experiments. The quasi-static simulation piercing forces of the graded core curves followed the main feature as in the virtual impact perforation curves. Virtual quasi-static tests of the intermediary's gradient profiles (E-4123 and D-2431) were also performed, and the results are shown in Figure 5(c) and (d), respectively. For all traces, an enhancement of the top skin piercing force on impact perforation was observed in comparison to the quasi-static ones. This enhancement is most probably related to the wave propagation effect inside the aluminum sheet. The piercing force level of the graded cores remained constant. Hence, quasi-static virtual perforation tests underestimate the perforation of the bottom skin for all graded core sandwich panels.
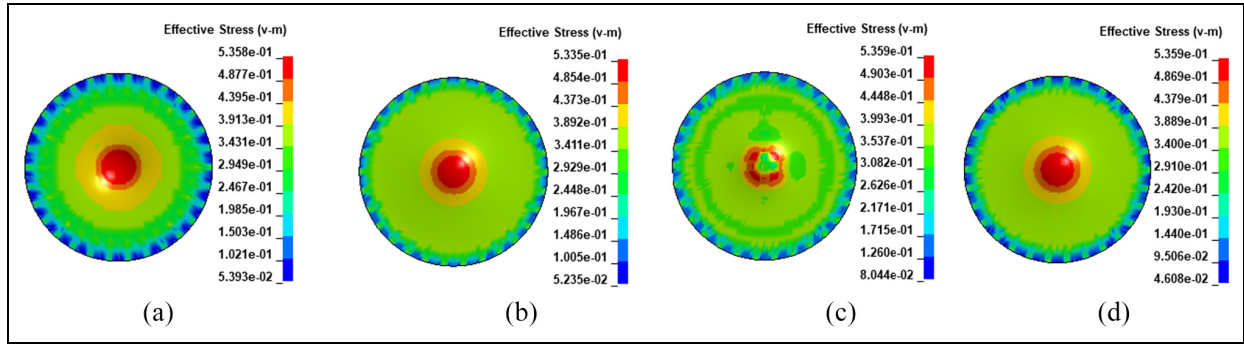
Figure 6. Contours of simulated effective von Mises stress [GPa] in the face sheets for graded core sandwich panels with different gradient profiles: (a) A-4321, (b) E-4123, (c) D-2431, and (d) B-1234.
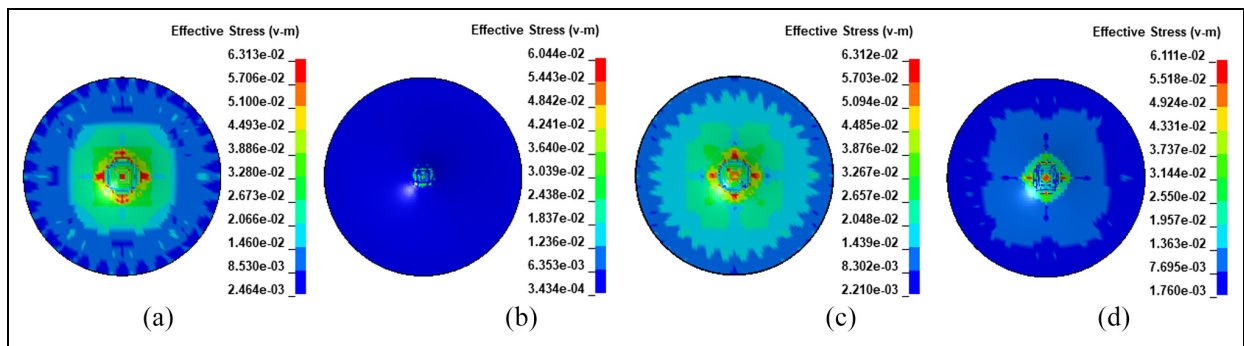

Figure 7. Contours of simulated effective von Mises stress [GPa] in the first layer for graded core sandwich panels with different gradient profiles: (a) A-4321, (b) E-4123, (c) D-2431, and (d) B-1234.

Analysis and discussion

Deformation and failure of the front face sheet

To assess how gradient profiles affect the impact perforation behavior of sandwich panels, simulated von Mises stress contours in the face sheet and the first core layers of A-4321, B-1234, E-4123, and D-2431 are plotted in Figures 6 and 7, respectively. These stress contours were taken at the moment just before failure in the front sheet. As can be observed, the stress contour was more concentrated around the impact region. It can also be seen that higher stress is generated in the front face sheet of A-4123, whereas B-1234 exhibits the lowest stress levels in the front face sheet. It was also observed that the stress contour is more concentrated around the edge of the indenter of the impact region for E-4123, despite being more concentrated beneath the indenter of the impact region for A-4321, B-1234, and D-2431. As illustrated in Figure 7(a), the stress contours in the graded cores indicate that high stress was mainly generated in the high-density layer.

Interestingly, the simulation was able to capture the petal-like failure mode in the experimental test for the top skin (Figure 8(a)) but could not capture the folding mode for the bottom skin (Figure 8(b)) in the A-4321
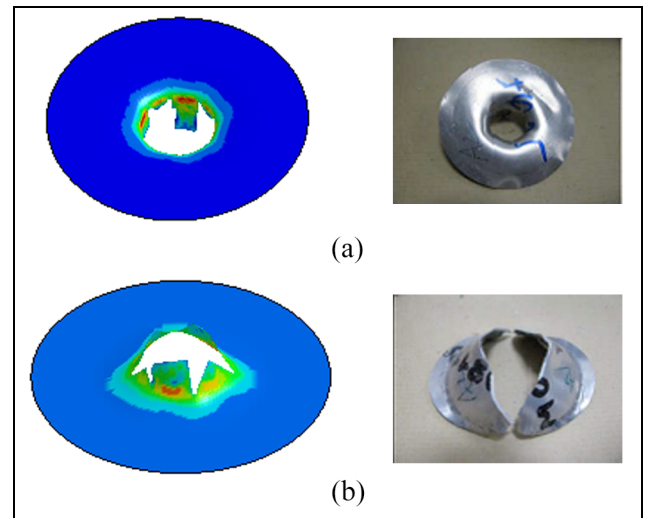

Figure 8. Breaking failure modes of the face sheets (top (a) and bottom (b) skins) by simulation and by postmortem observations for graded core sandwich panels with the gradient profile A-4321 (v = 45 m/s).[21]

gradient profile. This phenomenon is most probably due to the morphology of the hollow spheres, which makes it difficult for the numerical approach to
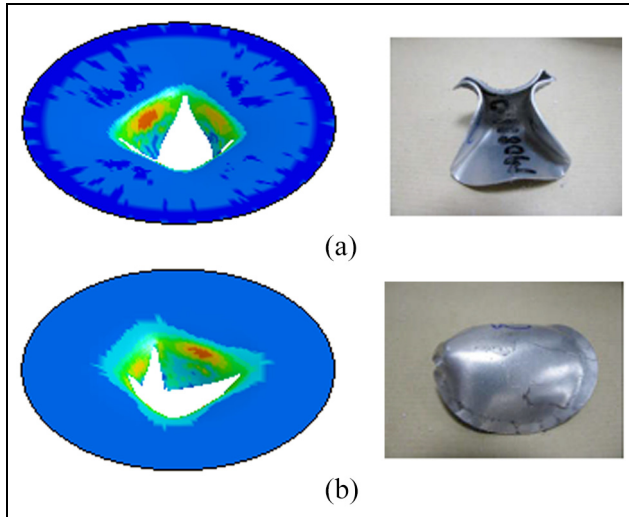
Figure 9. Breaking failure modes of the face sheets (top (a) and bottom (b) skins) by simulation and by post mortem observations for graded core sandwich panels with the gradient profile B-1234 (*v* = 45 m/s).[21]

Figure 11. Plots of simulated piercing force versus displacement for the impact perforation of homogenous core sandwich panels with different polymeric hollow sphere core densities (*v* = 45 m/s).
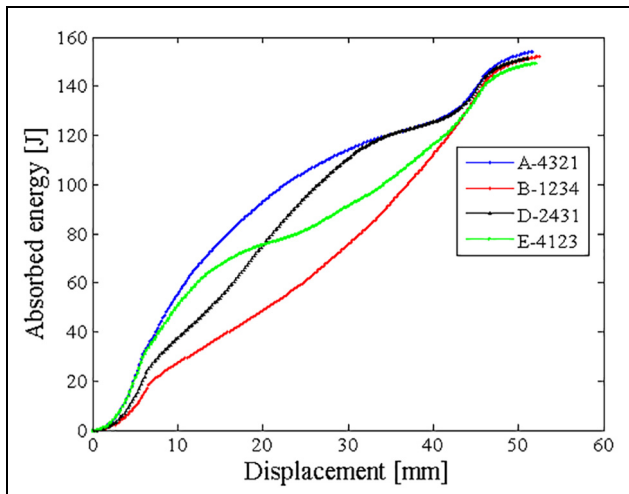

Figure 10. Plots of simulated absorbed energy versus displacement. Comparison between graded core sandwich panels with different gradient profiles (*v* = 45 m/s).

reproduce the failure feature of the bottom skin. It can also be seen that the failure modes of the top (Figure 9(a)) and bottom (Figure 9(b)) skin for the B-1234 gradient profile were different between the experimental and simulation tests because of the difference in the clumping boundary conditions.

Energy absorption characteristic

The energy required to perforate the graded core sandwich panels was calculated by determining the area under the piercing force–displacement curves. All sandwich panels with different layer configurations were
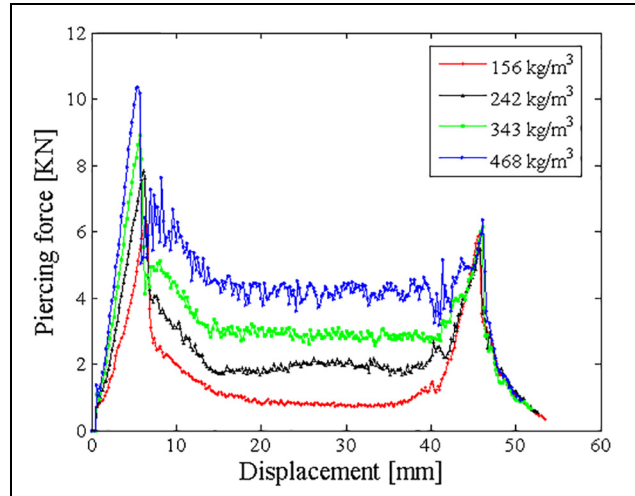
numerically tested under an impact of 803 J. Figure 10 compares the results in terms of the absorbed energy–displacement response. Importantly, the results show that graded core sandwich panels with a decreasing gradient profile (A-4321) outperform other core layer configurations in terms of energy absorption. In contrast, graded core sandwich panels with a linearly increasing gradient profile exhibit a weak energy absorption capacity. It can also be seen that the arrangement of the core layers has a weak influence on the energy absorption capacity, because the difference between the highest and the lowest energy absorption values is 5.1 J. This makes it difficult to enhance the energy capacity of sandwich panels by modifying the arrangement of the core layers.

It is very interesting to compare the perforation resistance of various graded hollow cores with that of similar sandwich panels based on a single type of core, such as sandwich panel construction. In this study, four single-type hollow spheres were taken as a reference: C1, C2, C3, and C4, with densities of 156, 242, 343, and 486 kg/m^{3}, respectively. Figure 11 shows the predicted perforation–displacement curves for these four ungraded sandwich panels. The results show that the perforation behavior of sandwich panels depends significantly on the strength of their core. Table 3 summarizes the peak forces for the perforation of the top and bottom skins and also shows the corresponding experimental results obtained by Zeng et al.[21] A good agreement was found between the simulation and experimental results for the three sandwiches (i.e. C1, C2, and C3), whereas a discrepancy was observed for the sandwich panel with a low-density core. Notably,

Table 3. Comparison of the top and bottom peak forces between the simulation and experimental results under an impact velocity of 45 m/s.

Sandwich	C1	C2	C3	C4
Core density (kg/m^3)	156	242	343	468
The first force peak force (N) Simulation data	6326	7830	8910	10350
The force peak force (N) Experimental data	–	8072	8978	11249
Error (%)	–	−2	−0.7	−7.9
The second peak force (N) Simulation data	5870	5480	6140	6330
The second peak force (N) Experimental data	–	6896	6301	6781
Error (%)	–	−20.5	−2.5	−6.6

Figure 13. Plots of piercing force versus displacement under impact loading at various velocities. Sandwich panels with the gradient profile A-4321.
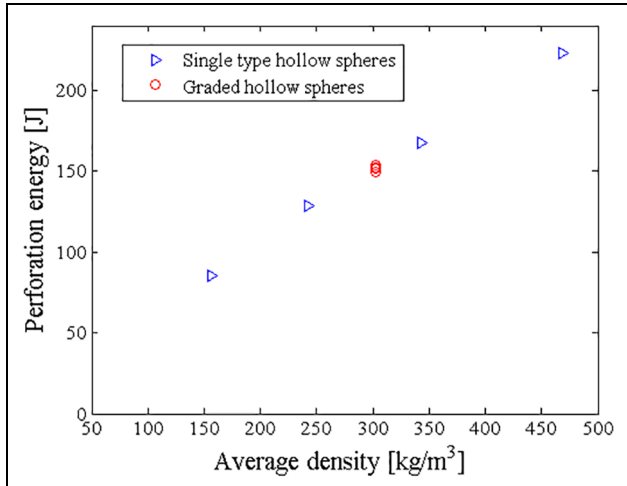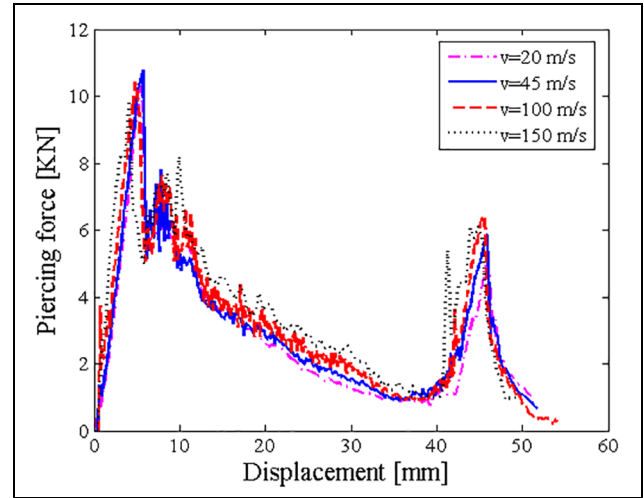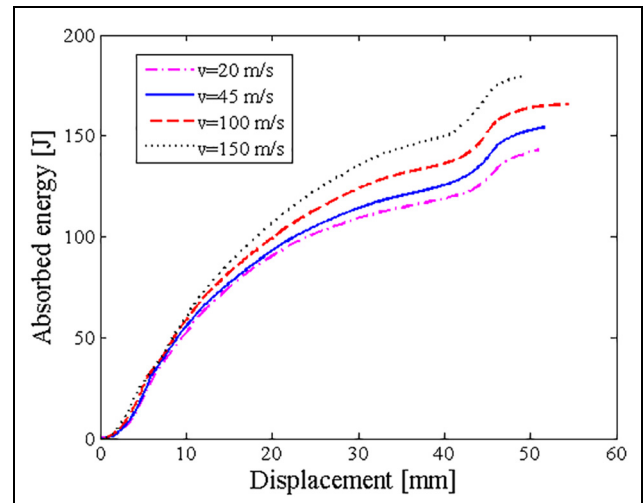

Figure 12. Comparison between the perforation energy and average density between different core layer arrangements and different single-type core sandwich panels (v = 45 m/s).

Figure 14. Plots of absorbed energy versus displacement under impact loading at various velocities. Sandwich panels with the gradient profile A-4321.

the top skin was not perforated in the experimental impact perforation test but was perforated in the virtual test. This phenomenon occurs most probably due to the difference between the experimental and numerical boundary conditions.

It was also interesting to compare the perforation energy capacity between graded core sandwich panels and sandwich panels with a single core. Figure 12 shows the predicted perforation energies and indicates that graded hollow core sandwich panels outperform sandwiches C1 and C2 and underperform sandwiches C3 and C4.

Effect of the loading rate

This numerical approach allows simulating tests at high impact velocities. Virtual graded core sandwich tests

were performed at velocities between 20 and 150 m/s. Figure 13 shows piercing force–displacement curves for different impact velocities. It can be seen that the incident top skin peak force is slightly decreased, whereas the piercing force–displacement curves for the layer cores were slightly increased with increasing impact velocity.

On the basis of the virtual force–displacement curves, the energies absorbed by the graded core sandwiches in each test are compared in Figure 14. Table 4 summarizes the absorbed energy for each virtual test at an impact velocity ranging from 20 to 150 m/s. The results also show that the absorbed energy is slightly
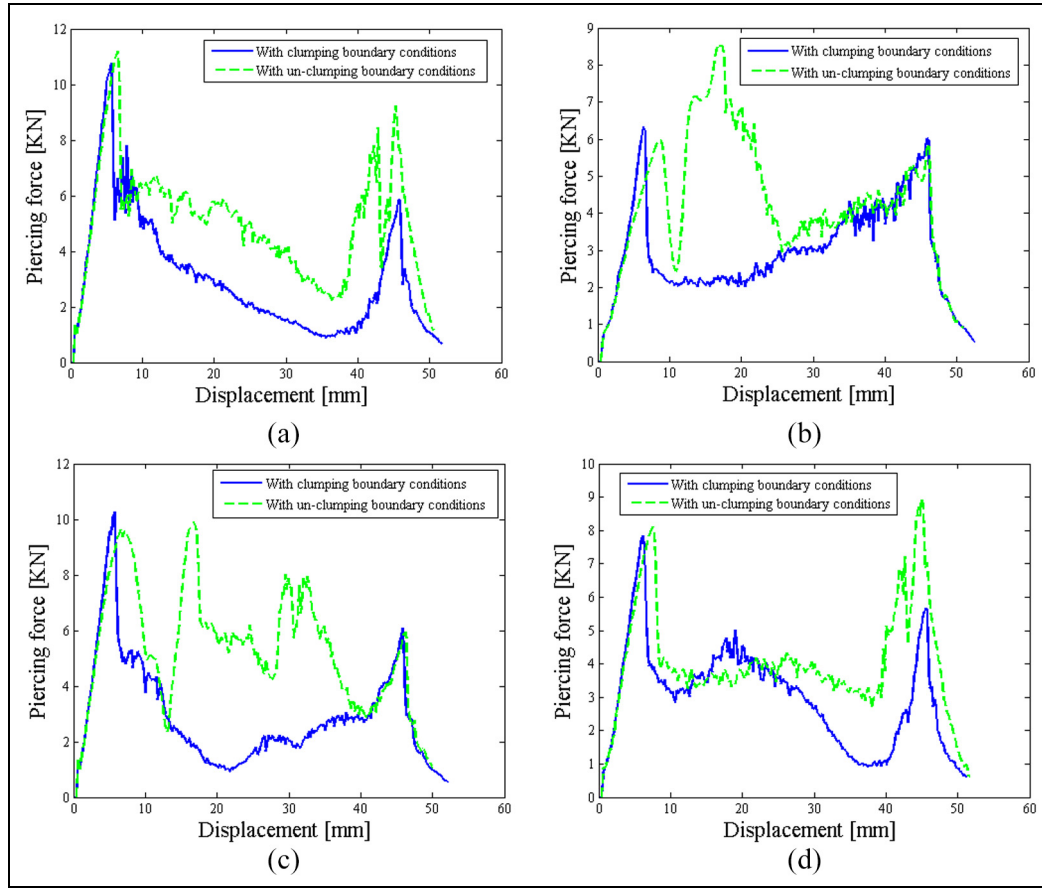
Figure 15. Plots of impact piercing force versus displacement for all graded core sandwich panels. Effect of boundary conditions. Sandwiches with the gradient profiles: (a) A-4321, (b) B-1234, (c) E-4123, and (d) D-2431.

Table 4. Prediction of the energy absorption at various impact velocities. Sandwich with the gradient profile: A-4321.

Impact velocity (m/s)	Energy absorbed (J)	Enhancement (%)
20	142.9	–
45	154.1	7.8
100	165.5	15.8
150	179.5	25.61

enhanced as the impact energy increases. This means that the effect of the core density gradient on the response of graded core sandwich panels is not significant when the impact energy increases. These results are consistent with those of Sun et al.[19] Such a small enhancement is most probably due to the small effect of shock front propagation inside the layers.[33]

Effect of the boundary conditions

To investigate the effect of the boundary conditions on the response of such graded core sandwich panels,

impact perforation without integrating a ring in the numerical approach was performed. For the sake of clarity, this numerical approach is called simulation with unclumping boundary conditions, whereas the first numerical approach is called simulation with clumping conditions (with a ring). The results are shown in Figure 15.

It can be seen that the boundary conditions significantly affect the overall response of graded core sandwich panels. It can also be observed that the weaker layer in all graded core sandwich panels has been crushed with the progression of the perforation process (see Figure 16). This means that this layer plays a dominant role in such an impact perforation process. Notably, in all sandwich panel gradient profiles, the piercing force of the layers was enhanced. The piercing top skin peak force remained constant for all sandwich gradient profiles, except for the case of graded core sandwich panel B-1234. Perforation of the top skin for this sandwich occurred after the first layer has been crushed. The deformation that occurred was found to be concentrated in the first layer, the strength of which determines whether the top skin will be perforated or
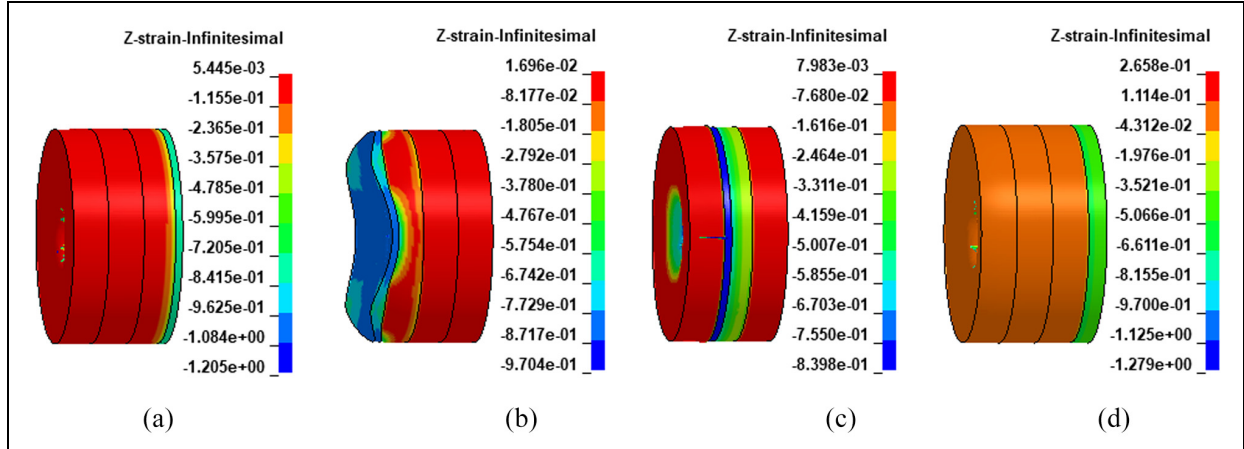
Figure 16. Deformation map for all graded core sandwich panels. Simulations under un-clumping boundary conditions (without a ring). Sandwiches with the gradient profiles: (a) A-4321, (b) B-1234, (c) E-4123, and (d) D-2431.

not. This can provide a good explanation for why the top skin peak force is high in the piercing force–displacement curve (Figure 15(b)). As illustrated in Figure 16(b), it can be seen that the top skin starts to fold concurrently with the compression of the weaker layer and then finally breaks in the petal-like mode. It was also observed that the bottom skin piercing peak force was enhanced for sandwiches with the gradient profiles A-4321 and D-2431, whereas it remained constant for sandwiches with the gradient profiles B-1234 and E-4123. This phenomenon occurs most probably as a result of the crushing of the weaker layer, which increases the strength of the layers and consequently leads to an increase in the level of the piercing forces. Such crushing was also well observed in the deformation map of the graded core sandwich panels with the gradient profiles A-4321, D-2431, and E-4123 (Figure 16(a), (c) and (d), respectively).

It was also interesting to observe how many of these structures can gain energy absorption when a fixed sandwich system is modified from clumping to unclumping boundary conditions. Figure 17 shows the energy absorbed versus displacement curves for these virtual impact perforation tests. An enhancement of the energy absorbed was observed in comparison to the results with clumping boundary conditions. Table 5 summarizes the predicted values of absorbed energy for both numerical approaches. The results indicate that the best strategy to enhance the energy absorption is to set un-clumping boundary conditions for the fixed sandwich system and to place the higher layer in contact with the top skin followed by the weaker layer as a second layer (i.e. graded sandwich panel with the gradient profile E-4123). These results suggest that the effect of the layer arrangement would be significant only if the boundary conditions of the graded core sandwich panels were of the un-clumping type.
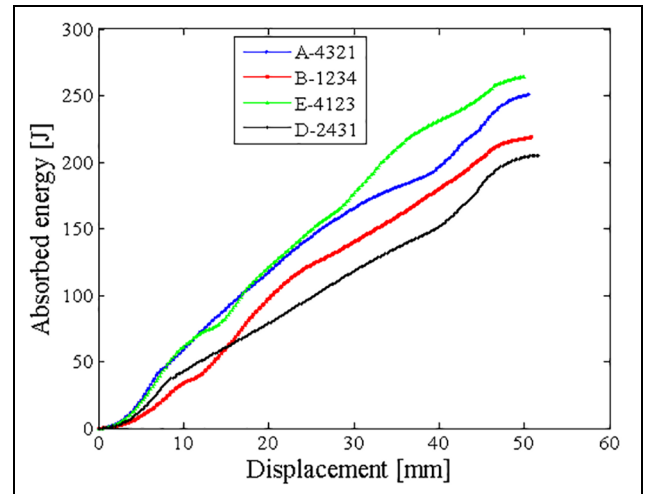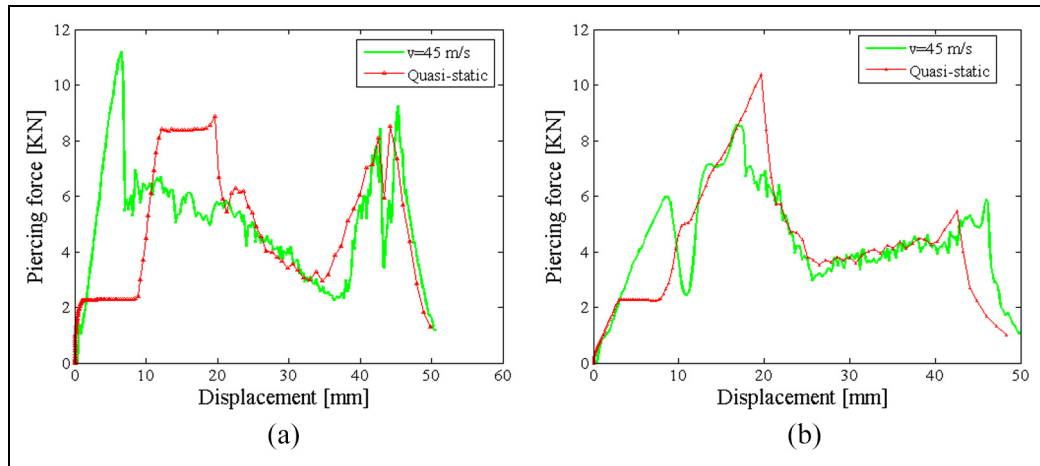

Figure 17. Plots of absorbed energy versus displacement under impact loading ($v = 45$ m/s) for all graded core sandwich panels under un-clumping boundary conditions (without a ring).

Virtual quasi-static perforation of graded sandwich panels with the gradient profiles A-4321 and B-1234 under un-clumping conditions was also performed. The results are shown in Figure 18(a) and (b), respectively, along with the results of the corresponding impact perforation. For A-4321, the results show two plateau forces corresponding to the crushing of the weaker layer first (Layer 1) and then the second layer (Layer 2). The top skin sheet was not pierced before a displacement of 20 mm (halfway). After this displacement, the force–displacement curve follows the same pattern as that of the corresponding impact perforation curve. For B-1234, the results show one plateau force corresponding to the crushing of the weaker layer (Layer 1). The top skin sheet was also not pierced before a displacement of 20 mm, and the peak force value was found

Table 5. Prediction of the energy absorption of the graded core sandwich under clumping and un-clumping boundary conditions.

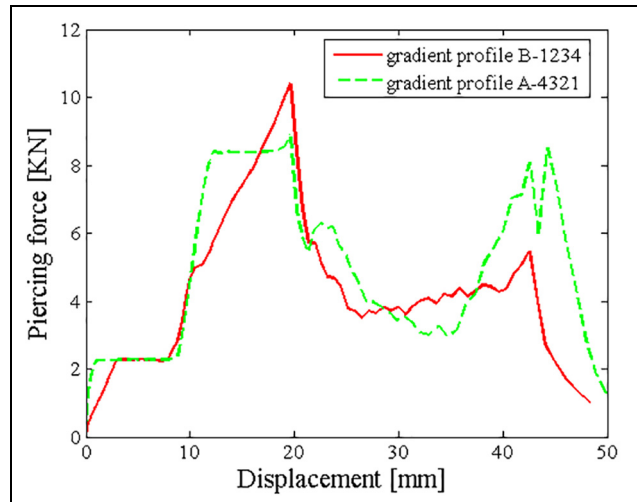| Sandwichs	Energy absorbed (J) clumping conditions	Energy absorbed (J) unclumping conditions	Enhancement %
A-4321	154.1	250.5	62.5
B-1234	152.1	218.6	43.7
D-2431	151.4	205.2	35.58
E-4123	149.2	264.2	77.1

Figure 18. Plots of impact and quasi-static piercing force versus displacement of graded core sandwich panels with the gradient profiles: (a) A-4321 and (b) B-1234.

to be higher than the impact peak value. After this displacement, the force–displacement curve follows the same pattern as that of the corresponding impact perforation curve. However, the breaking of the bottom skin sheet occurs at a displacement smaller than the impact perforation one.

From Figure 19, it can be seen that the piercing-displacement curves for the two gradient profiles are almost the same. This indicates that the gradient profiles have no effect on quasi-static perforation in the case of samples under un-clumping conditions. These results are consistent with the experimental results of Zeng et al.[21]

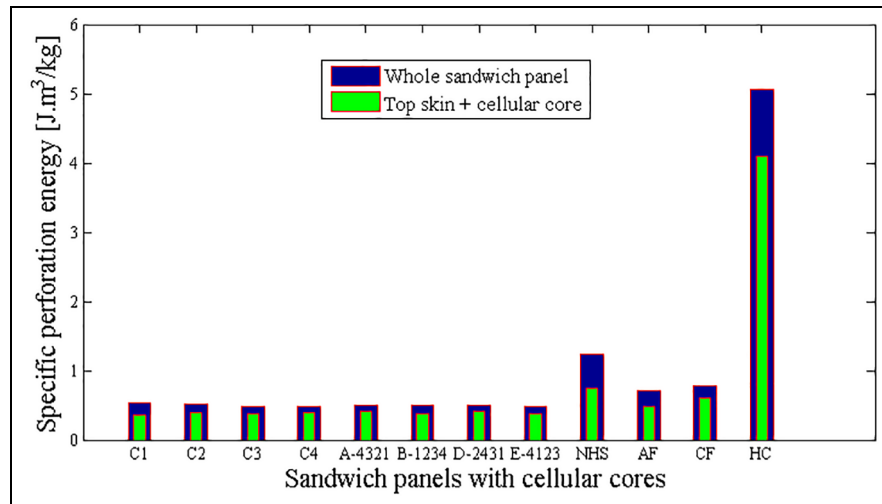### Comparison with other sandwich panel constructions

In the next stage of this investigation, the perforation resistance of various graded and homogenous hollow sphere core sandwich panels was compared with that of sandwich samples made of various cellular material cores (Cymat foam, Alporas foam, nickel hollow spheres, and 5056 honeycomb), with 0.8 mm thick 2024-T3 aluminum sheets as the top and bottom layers. Table 6 summarizes the properties of these different cellular material cores used in the sandwich panels.

Figure 19. Plots of quasi-static piercing force versus displacement of graded core sandwich panels with the gradient profiles A-4321 and B-1234 under un-clumping boundary conditions.

These sandwiches were tested under impact perforation of up to 46 m/s using the inverse perforation test setup. Notably, Zhao et al.[4] reported a significant enhancement of the top skin peak loads under perforation

Table 6. Cellular core configurations of the sandwich panels investigated in this study.

Code	Diameter/ length (mm^2)	Cellular core	Core density (kg/m^3)	Average sandwich mass (g)
C1	60×40	Ungraded Polymeric hollow spheres	156	38.75
C2	60×40	Ungraded Polymeric hollow spheres	242	50.1
C3	60×40	Ungraded Polymeric hollow spheres	343	56.42
C4	60×40	Ungraded Polymeric hollow spheres	468	69.37
A-4321	60×40	Graded polymeric hollow spheres	302	53.53
B-1234	60×40	Graded polymeric hollow spheres	302	53.53
D-2431	60×40	Graded polymeric hollow spheres	302	53.53
E-4123	60×40	Graded polymeric hollow spheres	302	53.53
NHS	60×40	Nickel hollow spheres[34]	185	36.9
AF	60×40	Alporas foam[34]	230	41.34
CF	60×40	Cymat foam[4]	235	43.7
HC	60×33	5056 Honeycomb[34]	38	20.3

Figure 20. Evaluation of the energy absorption capacity of graded and ungraded core sandwich panels with cellular cores (polymeric graded and ungraded hollow spheres, nickel hollow spheres, Alporas and Cymat foams, and 5056 honeycomb) normalized by the average core density to yield specific perforation values.

loading. This enhancement was attributed to the transient effect; the damage areas in the skin sheet is larger under impact loading which causes to a large deflection at fracturing. It should be noted that the perforation energies of these sandwich panels were calculated from the piercing–displacement traces recorded using the inverse perforation experimental setup. All perforation energies were calculated at almost the same impact velocity (43–45 m/s), which corresponds to an impact energy of 800 J. All perforation energies of the various sandwich panels were normalized by the average core density to obtain specific perforation values (see Figure 20). Normalizing the data in this way helped eliminate the effect of density. The results showed that the sandwich panel with a honeycomb core outperformed all the other sandwich panels, followed by the sandwich panel with a nickel hollow sphere core, that

with an aluminum Cymat core, and finally that with an aluminum Alporas foam core. However, sandwich panels with homogenous and graded polymeric hollow cores were found to be inferior to those with an Alporas foam core in terms of the specific energy capacity. The Figure 20 also indicates that the difference in specific perforation energy is not large between sandwich panels with homogenous polymeric hollow sphere and graded hollow sphere cores and between sandwich panels with Alporas and Cymat foam cores. It can also be seen that a large amount of energy was absorbed at a later phase during the perforation process for sandwich panels with honeycomb and nickel hollow sphere cores. This phenomenon occurs most probably as a result of the difference between the modes of failure of the perforation of the bottom skin. Indeed, the mode of failure of the bottom skin in these sandwich panels is

the folding process, which it absorbs more energy in comparison to the petal-like failure mode that occurs in other sandwich panels.

Conclusion

In this work, we numerically studied the impact perforation response of sandwich panels made of aluminum skins and graded polymeric hollow sphere cores. In total, four gradient profiles were taken as a reference in this study: A-4321, B-1234, D-2431, and E-4123. A suitable numerical model was conducted using the LS-DYNA code, calibrated using an inverse perforation test, instrumented with a pressure bar, and validated using experimental results reported in the literature.

The piercing force–displacement response, energy absorption, perforation resistance, and failure characteristics of these graded core sandwich panels were analyzed in detail. In addition, the effects of quasi-static and impact loading as well as the boundary conditions were studied. From the results and discussion, the following conclusions can be drawn:

(a) The numerical approach predicts with a high degree of accuracy the impact piercing force–displacement traces in the experimental test of graded core sandwich panels with decreasing gradient profiles (A-4321), whereas it fails to predict those of graded core sandwich panels with increasing gradient profiles (B-1234). The main reason for this is the difference in the boundary conditions between the numerical approach and the experimental test.

(b) The piercing force–displacement response of graded core sandwich panels is affected by the core density gradient profile. Graded core sandwich panels with decreasing gradient profiles (A-4321) have a strong top skin peak piercing force, whereas graded core sandwich panels with increasing gradient profiles (B-1234) have a weaker one.

(c) The absorbed energy of graded core sandwich panels is enhanced only under low-velocity perforation conditions ($< 45\,\text{m/s}$).

(d) The energy absorption capability of graded core sandwich panels can be effectively enhanced by modifying the arrangement of the core layers, but only under unclumping boundary conditions, which is hard to achieve with clumping boundary conditions. Sandwiches with an unbalanced V-shaped density profile with a gradient profile with more dense ends (E-4123) outperform other gradient profile configurations in terms of energy absorption, whereas sandwiches with an unbalanced

V-shape with a gradient profile with fewer dense ends (D-2431) exhibit the worst performance.

(e) The numerical approach developed here can capture the petal-like failure mode in the experimental test for the top skin, but it cannot capture the folding mode in the experimental test for the bottom skin.

(f) Gradient profiles have no effect on quasi-static perforation in the case of samples under unclumping conditions.

(g) A comparison of the specific perforation resistance of graded core sandwich panels with other sandwich panel constructions with different cellular material cores, such as nickel hollow spheres, Alporas and Cymat foam, and 5056 honeycomb, was provided.

ORCID iD

Ibrahim Elnasri https://orcid.org/0000-0002-1781-3038

References

1. Backman ME and Goldsmith W. The mechanics of penetration of projectiles into targets. *Int J Eng Sci* 1978; 16: 1–99.
2. Corbett GC, Reid SR and Johnson W. Impact loading of plates and shells by free flying projectiles: a review. *Int J Impact Eng* 1996; 18: 141–230.
3. Borvick T, Claussen AH, Hopperstad OS, et al. Perforation of AA5083-H116 aluminium plates with conical-nose steel projectles-experimental study. *Int J Impact Eng* 2004; 30: 367–384.
4. Zhao H, Elnasri I and Girard Y. Perforation of aluminium foam core sandwich panels under impact loading – an experimental study. *Int J Impact Eng* 2007; 34: 1246–1257.
5. Dean J, S-Fallah A, Brown PM, et al. Energy absorption during projectile perforation of lightweight sandwich panels with metallic fibre core. *Compos Struct* 2001; 93: 1089–1095.
6. Pattofatto S, Zeng HB and Zhao H. On the piercing force enhancement of aluminium foam sandwich plates under impact loading. *J Sandw Struct Mater* 2011; 14: 687–697.
7. Elnasri I and Zhao H. Impact perforation of sandwich panels with aluminum foam core: a numerical and analytical study. *Int J Impact Eng* 2016; 96: 50–60.

8. Concli F, Gonzalez-Jimenez A, Manes A, et al. Experimental testing and numerical modelling of a Kevlar woven - Epoxy matrix composite subjected to a punch test. *Procedia Struct Integrity* 2019; 24: 3–10.

9. Berk B, Karakuzu R and Toksoy AK. An experimental and numerical investigation on ballistic performance of advanced composites. *J Compos Mater* 2017; 51: 3467–3480.

10. Bresciani LM, Manes A, Ruggiero A, et al. Experimental tests and numerical modelling of ballistic impacts against Kevlar 29 plain-woven fabrics with an epoxy matrix: macro-homogeneous and meso-heterogeneous approaches. *Compos Part B: Eng* 2016: 88: 114–130.

11. Gama BA and Gillespie JW Jr. Punch shear based penetration model of ballistic impact of thick-section composites. *Compos Struct* 2008; 86: 356–369.

12. Venkataraman S and Sankar BV. Elasticity solution for stresses in a sandwich beam with functionally graded core. *AIAA* 2003; 41: 2501–2505.

13. Suresh S and Mortensen A. *Fundamentals of functionally graded materials*. London: The Institute of Materials, 1998.

14. Butcher RJ, Rousseay CE and Tippur HV. A functionally graded particulate composite: preparation, measurements and failure analysis. *Acta Mater* 1998; 47: 259–268.

15. Parameswaran V and Shukla A. Processing and characterization of a model functionally gradient material. *J Mater Sci* 2000; 35: 21–29.

16. Etemadi E, Khatibi AA and Takaffoli M. 3D finite element simulation of sandwich panels with a functionally graded core subjected to low velocity impact. *Compos Struct* 2009; 89: 28–34.

17. Zhou J, Guan ZW and Cantwell WJ. The impact response of graded foam sandwich structures. *Eng Struct* 2013; 97: 370–377.

18. Jing J, Yang F and Zhao L. Perforation resistance of sandwich panels with layered gradient metallic foam cores. *Eng Struct* 2017; 171: 217–228.

19. Sun G, Wang E, Wanf H, et al. Low-velocity impact behaviour of sandwich panels with homogeneous and stepwise graded foam cores. *Mater Des* 2018; 160: 1117–1136.

20. Baba BO. Curved sandwich composites with layer-wise graded cores under impact loads. *Eng Struct* 2017; 159: 1–11.

21. Zeng HB, Pattofatto, Zhao H, et al. Perforation of sandwich plates with graded hollow sphere cores under impact loading. *Int J Impact Eng* 2010; 37: 1083–1091.

22. Hohe J, Hardenacke V, Fascio V, et al. Numerical and experimental design of graded cellular sandwich cores for multi-functional aerospace applications. *Mater Des* 2012; 39: 20–32.

23. Zeng HB, Pattofatto S, Zhao H, et al. Impact behaviour of hollow sphere agglomerates with density gradient. *Int J Mech Sci* 2010; 52: 680–688.

24. Liu Y, Wu HX and Wang B. Gradient design of metal hollow sphere (MHS) foams with density gradients. *Compos Part B* 2012; 43: 1346–1352.

25. Chen C, Yu T and Lu G. A double shock mode in graded cellular rod under impact. *Int J Solids Struct* 2013; 50: 217–233.

26. Zhang J, Zhang Y, Fan J, et al. Mesoscopic investigation of layered graded metallic foams under dynamic compaction. *Adv Struct Eng* 2018; 21: 2081–2098.

27. Lui J, Hou B, Lu F, et al. A theoretical study of shock front propagation in the density graded cellular rods. *Int J Impact Eng* 2015; 80: 133–142.

28. Duan Y, Zhao X, Liu Z, et al. Dynamic response of additively manufactured graded foams. *Compos Part B* 2020; 183: 107630.

29. Duan Y, Zhao X, Du B, et al. Quasi-static compressive behavior and constitutive model of graded foams. *Int J Mech Sci* 2020; 177: 105603.

30. Lemaitre J. *A course on damage mechanics*. 2nd ed. Berlin: Springer, 1996.

31. Hallquist JO. *Theoretical manual*. Livermore, CA: Livermore Software Technology Corporation, 1998.

32. Hanssen AG, Hopperstad OS, Langsethand M, et al. Validation of constitutive models applicable for aluminium foams. *Int J Mech Sci* 2002; 44: 359–406.

33. Elnasri I, Pattofatto S, Zhao H, et al. Shock enhancement of cellular structures under impact loading: part I experiments. *J Mech Phys Solids* 2007; 55: 2652–2671.

34. Elnasri I. *Comportement des matériaux cellulaires sous impact et de panneaux sandwichs sous perforation dynamique*. PhD Thesis, Ecole normale supérieure de Cachan, Fr, 2006.